Optical second-harmonic spectroscopy of Au(887) and Au(443) surfaces

Yojiro Maeda, Tetsuya Iwai, Yoshihiko Satake, Keishi Fujii, Shigeru Miyatake, Daisuke Miyazaki, and Goro Mizutani*
School of Materials Science, Japan Advanced Institute of Science and Technology 1-1 Asahidai, Nomi, Ishikawa 923-1292, Japan

(Received 20 May 2008; revised manuscript received 21 July 2008; published 27 August 2008)

In order to investigate the electronic states of step sites on Au surfaces, we have observed the reflected optical second-harmonic (SH) intensity from Au(887) and Au(443) surfaces in ultrahigh vacuum with a normal incident excitation light beam, as a function of the photon energy and the incident and SH light polarizations. The second-order surface nonlinear susceptibility elements observed in this measurement configuration were $\chi^{(2)}_{xxx}$, $\chi^{(2)}_{xyy}$, and $\chi^{(2)}_{yxy}$, where x and y are defined as the $[11\bar{2}]$ and $[\bar{1}10]$ directions, respectively. The step edges lie in the y direction. The ratios of the nonlinear susceptibility elements $|\chi^{(2)}_{xyy}|/|\chi^{(2)}_{xxx}|$ and $|\chi^{(2)}_{yxy}|/|\chi^{(2)}_{xxx}|$ were different on the two surfaces in the photon energy range from $2\hbar\omega=2.5$ to 3.3 eV. The deviation of the SH response from that of an ideal $3m$ symmetric Au(111) surface was found to be larger for the Au(443) surface than for the Au(887) surface. This deviation is attributed to the atomic steps created by the miscut of the samples. In order to analyze the observed SH spectra, we calculated the electronic states of a Au(554) slab using a density-functional theory. We found that the low-energy onset of the SH intensity caused by the steps can be qualitatively interpreted by referring to the calculated partial density of the d-electronic states of the step and terrace atoms on the Au slab.

DOI: 10.1103/PhysRevB.78.075440 PACS number(s): 78.68.+m, 78.66.Bz, 73.21.−b, 42.65.Ky

I. INTRODUCTION

Both the response of free electrons in a positive background (the jellium model) and that of localized electrons near the metal atoms should be considered in the interpretation of electronic phenomena in metals. The chemisorption of atoms and molecules is a typical phenomenon on solid-state surfaces; on noble metal surfaces it is thought to involve d electrons.[1] However, in the example of hydrogen adsorption on the surface of the familiar noble metal Au, the H-Au bond is not stable due to the occurrence of antibonding electronic orbitals. These orbitals consist of hydrogen 1s and Au 5d-electronic wave functions just below the Fermi energy. This is why Au is the most inert of the noble metals and it rarely adsorbs atoms or molecules on its surface.

On the other hand, it has been found that chemisorption selectively occurs at defects or step sites on Au surfaces.[2] It has been shown experimentally that the π^*(CO)-d(Au) bond of the adsorbed CO molecules on the steps is stronger than the one on the terraces. This fact suggests that the electronic states near the steps are quite different from those in the middle of the terraces. Thus it is essential to analyze the local electronic structures around the steps in order to clarify the mechanism of real surface reactions on the Au surface.

Recently Au has been found to have a considerable catalytic ability to oxidize CO into CO_2 when it is supported on a TiO_2 substrate as nanoparticles, as reported by Valden and co-workers.[3–5] Au nanoparticles become insulators when their sizes are smaller than a certain threshold. At the same sizes, they become catalytically reactive. This fact suggests that there could be a correlation between the catalytic function and the electronic structure of the nanosized Au particles.

Several possible origins of this catalytic activity of the Au particles have been proposed. They are (1) coordinative unsaturation of the surface atoms, (2) active sites at the Au/TiO_2 support interface, (3) reactivity of small gold particles due to quantum size effects, and (4) the nanosized structures, such as steps or kinks formed at the surfaces of the Au nanoparticles.[6] Determining the most feasible of these candidates to explain the origin of the CO oxidation is still considered to be an important topic of discussion.

In this study, as a possible step in determining the origin of the catalytic activity of Au nanoparticles, we have focused on candidate (4) above, namely, the nanosized structures on Au surfaces or interfaces, especially the electronic states of the step sites. In a previous study of the electronic states of stepped Au surfaces, Ortega *et al.*[7] and other researchers investigated vicinal Au(111) surfaces by angle-resolved photoemission spectroscopy. They reported that the electronic states show one-dimensional levels, due to the confinement of electrons on the terraces between the steps. Shiraki *et al.* deposited Fe on a Au(887) surface and found that the Fe atoms are preferentially adsorbed at the step sites, reducing the step barrier potential. With this reduction in the step barrier potential, electron propagation across the decorated steps on the vicinal surfaces became more free-electron-like.[8] These results suggest that the electronic structure of bare step atoms is different from that of terrace atoms. However, neither paper reported on the electronic spectra of the steps. So far, as we know, there has been no measurement of the energy spectrum of the electronic structure of the step sites on Au.

We chose high index Au surfaces, Au(443) and Au(887), as our samples and analyzed their electronic structure by optical second-harmonic (SH) spectroscopy. The surfaces of Au(443) and Au(887) are tilted from the Au(111) plane in the $[11\bar{2}]$ direction by 7.2° and 3.5°, respectively. These vicinal Au(111) surfaces consist of atomic steps separated by (111) terraces. For Au(775) tilted by 8.5° from Au(111), it has been reported that step bunching occurs and the surface has a phase separation into two kinds of vicinals.[9] The Au(443)

surface is tilted only a little less than Au(775) so we expect that the phase separation and step bunching occurs in a similar fashion. On the other hand, it has been reported that step bunching does not occur on Au(887) and a single phase of vicinals was observed.[8,10]

Optical second-harmonic generation (SHG) is forbidden in centrosymmetric bulk media and occurs only at their surfaces.[11] Janz *et al.*[12] performed SHG measurements of vicinal Al(100) surfaces at several incident angles and have detected a SH response from the steps. In an experiment involving the normal incidence of a centrosymmetric medium, similar to the one in this study, SHG occurs only if there is asymmetry in the two-dimensional surface plane; so it is more advantageous to detect the signal from the steps.

In the Au(111) terrace the top atomic layer alone has $6/mmm$ symmetry and is centrosymmetric. However, the incorporation of the second and third atomic layers yields $3m$ symmetry and loss of the center of inversion. Vicinal Au(111) surfaces, such as Au(443) and Au(887), have ordered surface steps with faces oriented in the $[11\bar{2}]$ direction, and these oriented steps add further asymmetry in the surface plane. On the terraces of the Au surfaces tilted from the (111) surface in the $[11\bar{2}]$ direction, structures known as discommensuration lines caused by the $\sqrt{3}\times 23$ reconstruction are reportedly formed.[8,13] This $\sqrt{3}\times 23$ reconstruction also adds asymmetry in the $[11\bar{2}]$ direction. The additional asymmetry caused by both the step structures and the reconstruction is expected to modify the SH response.

Since the structures of the Au(443) and Au(887) surfaces have m symmetry with a mirror plane normal to the $[\bar{1}10]$ direction, they have nonzero second-order nonlinear susceptibility elements $\chi^{(2)}_{xxx}$, $\chi^{(2)}_{xxz}$, $\chi^{(2)}_{xyy}$, $\chi^{(2)}_{xzz}$, $\chi^{(2)}_{yxy}$, $\chi^{(2)}_{yyz}$, $\chi^{(2)}_{zxx}$, $\chi^{(2)}_{zxz}$, $\chi^{(2)}_{zyy}$, and $\chi^{(2)}_{zzz}$. Here the x, y, and z axes are defined to lie in the $[11\bar{2}]$, $[\bar{1}10]$, and $[111]$ directions, respectively. The step faces and substrate normal lie in the y and z directions, respectively.

For normal incidence onto this surface, SH light occurs due to the $\chi^{(2)}_{xxx}$, $\chi^{(2)}_{xyy}$, and $\chi^{(2)}_{yxy}$ elements. The SH response for normal incidence from the Au(111) surface with $3m$ symmetry is generated by the same nonlinear susceptibility elements but with an additional relation, as discussed in Ref. 14;

$$\chi^{(2)}_{xxx}:\chi^{(2)}_{xyy}:\chi^{(2)}_{yxy} = 1:-1:-1. \tag{1}$$

The SH response arises from the sum of the nonlinear susceptibility,

$$\chi^{(2)}_{3m} + \chi^{(2)}_{\mathrm{asym}}, \tag{2}$$

where $\chi^{(2)}_{3m}$ and $\chi^{(2)}_{\mathrm{asym}}$ represent the nonlinear susceptibility originating from the $3m$ symmetric surface and the asymmetric structures such as steps or reconstructed terraces, respectively. The resonant deviation of the SH intensity pattern from the $3m$ symmetry as a function of the photon energy thus observed is expected to reflect the electronic level at the asymmetric site.

The Au(443) surface has greater step density than the Au(887) surface. In contrast, the Au(887) surface has a larger area of reconstructed terraces than the Au(443) surface. This is because the reconstruction does not occur on the narrow terraces of the Au(443) surface.[7,9] We expect the SH response due to the asymmetry of the steps to be stronger for Au(443), while that of the reconstruction should be stronger for Au(887).

In our results, the deviation of the SH response from that of $3m$ symmetric Au(111) was stronger for Au(443) than for Au(887), indicating that the SH response due to the additional asymmetry originates with the steps. Thus, we can consider SHG information for the stepped surfaces to be fundamental for understanding the catalytic activity of Au nanostructures.

II. EXPERIMENT

The samples were mechanically polished Au(443) and Au(887) disks (Surface Preparation Laboratory) mounted as delivered in an ultrahigh vacuum chamber with a base pressure at around 2.5×10^{-8} Pa. After five repetitions of annealing at 500 °C by flash heating and sputtering by Ar^+ ions of 0.5 keV, annealing was done once more at the end of the cleaning. There was no contamination on the Au surfaces thus prepared, as checked by Auger electron spectroscopy (AES). This cleanliness was confirmed to be maintained for at least 8 h at room temperature, and our SH spectroscopy of the Au surfaces was carried out within 8 h after cleaning.

In order to characterize the Au surface structures, a reflection high-energy electron diffraction (RHEED) was observed with an incident electron energy of 15 keV and the beam direction parallel to $[\bar{1}10]$. As a result of step bunching, the RHEED pattern of the Au(443) surface showed two kinds of satellite streaks corresponding to two different terrace widths, in addition to the main streaks. The terrace widths were estimated to be 1.4 ± 0.1 and 3.4 ± 0.3 nm. On the wider terraces $\sqrt{3}\times 23$ reconstruction occurred with the $\times 23$ periodicity in the $[\bar{1}10]$ direction. On the narrower terraces the $\sqrt{3}\times 23$ reconstruction was not observed by scanning tunnel microscope (STM).[9,15] On the other hand, the Au(887) surface was found to be a single domain structure of 3.8 ± 0.4 nm width terraces with $\sqrt{3}\times 23$ reconstruction. The orientation of the Au samples was adjusted for optical measurement using the RHEED patterns.

Figure 1 diagrams the experimental setup for the SHG measurements used in this study. The light source of the fundamental frequency was an optical parametric oscillator (Spectra Physics MOPO-730) driven by a frequency-tripled Q-switched Nd:YAG (yttrium aluminum garnet) laser. The laser power was 1.5 mJ/pulse with a duration of 3 ns and a repetition rate of 10 Hz. The incident beam was passed through a dichroic mirror (YHS-50-C08–355, DIF-50S-RED) and focused into a 3-mm diameter spot on the Au sample surface with a normal incident angle. The reflected SH light beam in the normal direction was reflected selectively by the dichroic mirror, passed through an ω cut filter, a polarizer, lenses, and a monochromator, and finally was detected by a photomultiplier. To compensate for the temporal

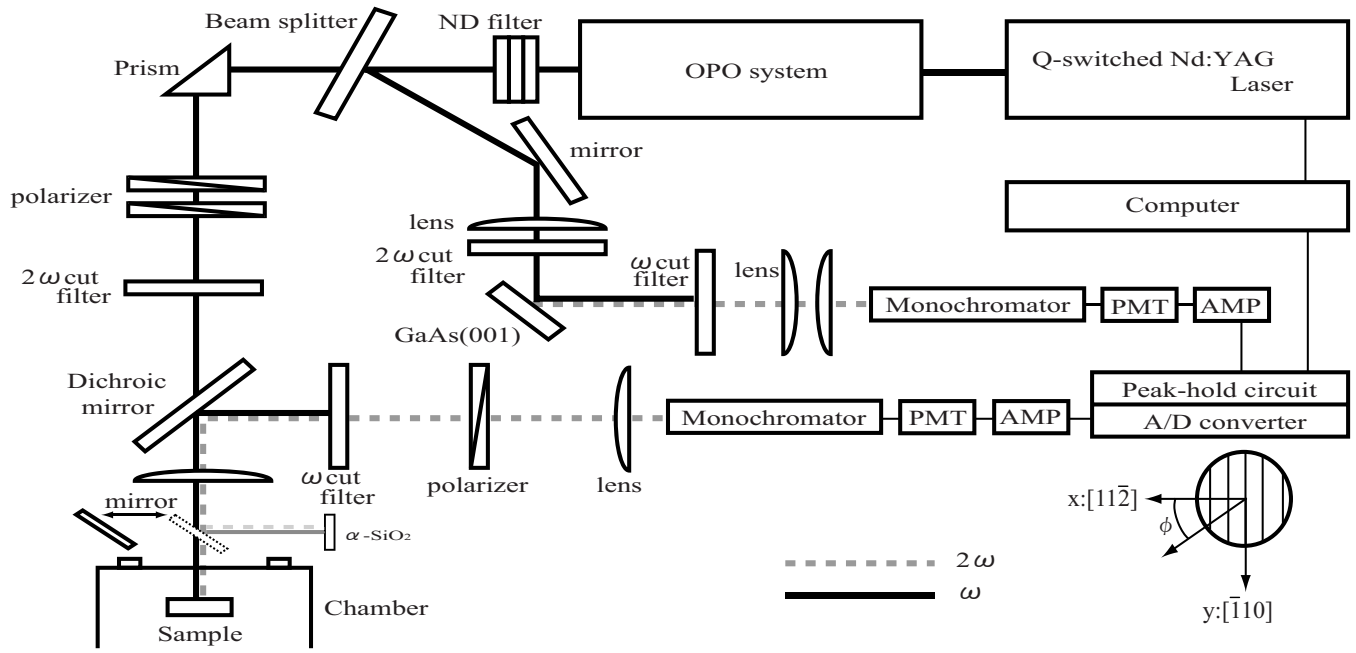

FIG. 1. Block diagram of the SHG measurement system. The laboratory coordinates x and y on the sample surface are defined in the inset in the lower part of the figure. The angle ϕ is defined as the angle between the $[11\bar{2}]$ direction and incident polarization. PMT: photomultiplier, AMP: amplifier, and OPO: optical parametric oscillator.

variation of the incident laser pulse power, we used a reference sample [GaAs(001) in air] and calibrated the signal intensity by taking the ratio of the intensities measured in the signal and reference channels. To compensate for the sensitivity variation of the optical system as a function of the SH photon energy, a sliding mechanism inserted a mirror into the optical path and the SH intensity was measured at each wavelength by the reflected beam from an α-SiO_2(0001) plate. The SH intensity from the Au samples was calibrated by that from this reference α-SiO_2(0001) plate.

The incident polarization angle ϕ of the excitation beam is defined as the angle between the direction of the electronic field of light and the $[11\bar{2}]$ direction of the Au crystals. When measuring the SH intensity as a function of ϕ, the observed polarization of the SH light was set at either 0° or 90° and the measurement was done for every 10° of ϕ. When measuring the SH intensity as a function of the photon energy, the observed polarization of the excitation beam was set at ϕ=0°, 45°, or 90° and the polarization of the SH light was set at 0° or 90°. The ratios of the SH intensity with these values to that with ϕ=0° incidence and SH polarization angle 0° was measured as a function of the photon energy. When measuring the absolute SH intensity spectra normalized by using the α-SiO_2(0001) reference sample, the excitation beam was set at ϕ=0° and the SH light polarization was set at 0°.

III. RESULTS AND DISCUSSION

Figure 2 shows the SH intensity patterns from the Au(443) sample as a function of the incident polarization angle ϕ. The SH photon energy was 2.7 eV and the observed polarization of the SH light was fixed at 0° for $I^{(2\omega)}_{\mathrm{exp},x}(\phi)$ in Fig. 2(a) and 90° for $I^{(2\omega)}_{\mathrm{exp},y}(\phi)$ in Fig. 2(b). We see four lobes in each pattern but the incident polarization angles giving the SH intensity maxima are different in Figs. 2(a) and 2(b). Phenomenologically the SH intensity is written as

$$I_x^{(2\omega)}(\phi) = C^2 I^{(\omega)^2}\left\{|\chi^{(2)}_{xxx}|^2 \cos^4\phi + |\chi^{(2)}_{xyy}|^2 \sin^4\phi + \frac{1}{2}\mathrm{Re}(\chi^{(2)}_{xxx}\chi^{(2)*}_{xyy})\sin^2 2\phi\right\}, \quad (3)$$

for the pattern in Fig. 2(a) and

$$I_y^{(2\omega)}(\phi) = C^2 I^{(\omega)^2}|\chi^{(2)}_{yxy}|^2 \sin^2 2\phi, \quad (4)$$

for that in Fig. 2(b).Here C is a coefficient defined as $|F(2\omega)F(\omega)^2|=C$, where $F(\omega)$ is a linear Fresnel factor and

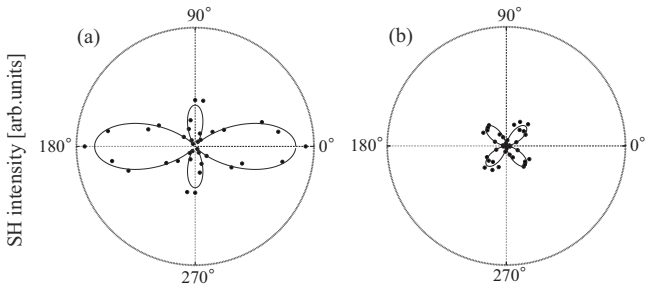

FIG. 2. SH intensity from Au(443) as a function of the angle ϕ of the polarization of the incident beam at SH photon energy of 2.7 eV. The observed polarization angle of the SH light is (a) 0° and (b) 90°. The solid curves in (a) and (b) are least-square-fitted curves to the experimental data using Eqs. (3) and (4). The SH intensity is in an arbitrary unit on a common scale in the two patterns.

$F(2\omega)$ is a second-order Fresnel factor.[16] The difference between the Fresnel factors of Au(887) and Au(443) is very small because their linear dielectric constants are nearly the same. Comparing the SH intensity patterns $I^{(2\omega)}_{\mathrm{exp},x}(\phi)$ and $I^{(2\omega)}_{\mathrm{exp},y}(\phi)$ in Figs. 2(a) and 2(b) with $I^{(2\omega)}_{x}(\phi)$ and $I^{(2\omega)}_{y}(\phi)$ in Eqs. (3) and (4), respectively, we have obtained the ratios of the absolute values of the nonlinear susceptibility elements as

$$|\chi^{(2)}_{xxx}|:|\chi^{(2)}_{xyy}|:|\chi^{(2)}_{yxy}| = 1:0.89:0.66, \tag{5}$$

at a photon energy of $2\hbar\omega=2.7$ eV. From Eq. (1), the $3m$ symmetric Au(111) surface will give the ratios as in Ref. 14:

$$|\chi^{(2)}_{xxx}|:|\chi^{(2)}_{xyy}|:|\chi^{(2)}_{yxy}| = 1:1:1. \tag{6}$$

The values of $|\chi^{(2)}_{xyy}|/|\chi^{(2)}_{xxx}|=0.89$ and $|\chi^{(2)}_{yxy}|/|\chi^{(2)}_{xxx}|=0.66$ for Au(443) in Eq. (5) are both smaller than $|\chi^{(2)}_{xyy}|/|\chi^{(2)}_{xxx}|=1$ and $|\chi^{(2)}_{yxy}|/|\chi^{(2)}_{xxx}|=1$ for the $3m$ symmetric Au(111) surface in Eq. (6). Solid curves in Figs. 2(a) and 2(b) are least-square-fitted curves to the experimental data using Eqs. (3) and (4), where the phase difference $(\beta-\alpha)$ between the susceptibility elements $\chi^{(2)}_{xxx}$ and $\chi^{(2)}_{xyy}$ is also a fitting parameter. We define the phase difference as $(\beta-\alpha)$, rewriting the two susceptibility elements as $\chi^{(2)}_{xxx}=|\chi^{(2)}_{xxx}|e^{-i\alpha}$ and $\chi^{(2)}_{xyy}=|\chi^{(2)}_{xyy}|e^{-i\beta}$. As mentioned in the introduction, both the step structures and the reconstruction on the terraces give asymmetry in the x direction on the Au(443) surface. The difference in the SH intensity patterns of Au(887) and Au(443) compared to that of Au(111) are due to either the steps or the reconstruction.

Figure 3 shows the SH intensity ratios $I^{(2\omega)}_{\mathrm{exp},x}(\phi=90°)/I^{(2\omega)}_{\mathrm{exp},x}(\phi=0°)$ and $I^{(2\omega)}_{\mathrm{exp},y}(\phi=45°)/I^{(2\omega)}_{\mathrm{exp},x}(\phi=0°)$ as a function of the SH photon energy. Dots indicate Au(887) and empty circles are for Au(443). The difference in the SH responses of Au(887) and Au(443) is clearly seen in the SH photon energy range from 2.5 to 3.3 eV.

From Eq. (3) the vertical axis in Fig. 3(a) is found to be

$$I^{(2\omega)}_{\mathrm{exp},x}(\phi=90°)/I^{(2\omega)}_{\mathrm{exp},x}(\phi=0°) = \frac{|\chi^{(2)}_{xyy}|^2}{|\chi^{(2)}_{xxx}|^2}, \tag{7}$$

and that in Fig. 3(b) is found to be

$$I^{(2\omega)}_{\mathrm{exp},y}(\phi=45°)/I^{(2\omega)}_{\mathrm{exp},x}(\phi=0°) = \frac{|\chi^{(2)}_{yxy}|^2}{|\chi^{(2)}_{xxx}|^2}. \tag{8}$$

According to Eq. (6) the SH intensity ratios, Eqs. (6) and (7), are unity for $3m$ symmetric Au(111). The SH intensity ratios observed in Fig. 3 indicate that the ratios of the nonlinear susceptibility elements $|\chi^{(2)}_{xyy}|/|\chi^{(2)}_{xxx}|$ and $|\chi^{(2)}_{yxy}|/|\chi^{(2)}_{xxx}|$ for Au(887) are closer to unity than those for Au(443) in the SH photon energy range from 2.5 to 3.3 eV.

As was already mentioned, the Au(443) surface has two kinds of terraces. Long terraces have a width of about 3.4 ± 0.3 nm, while narrow terraces have a width of about 1.4 ± 0.1 nm. Because reconstruction does not occur on the narrow terraces of Au(443), the total area of reconstruction is larger for Au(887). Thus the effect of the broken symmetry by $\sqrt{3}\times23$ reconstruction should be greater for Au(887) than for Au(443). However, in Fig. 3 the deviation of the SH intensity ratios from unity are larger for Au(443). Therefore, the effect of the reconstruction on SH intensity cannot be regarded as dominant.

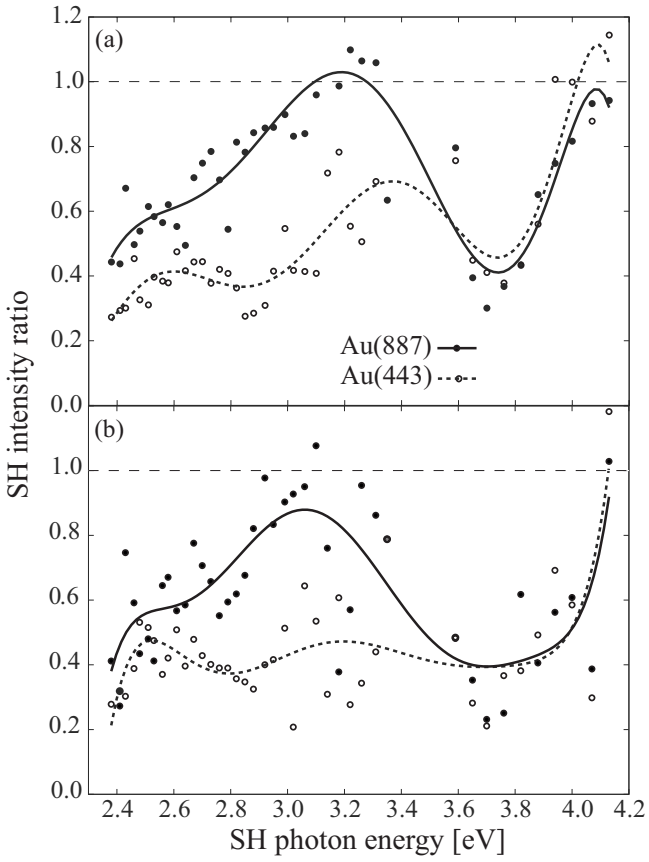

FIG. 3. SH intensity ratios (a) $I^{(2\omega)}_{\mathrm{exp},x}(\phi=90°)/I^{(2\omega)}_{\mathrm{exp},x}(\phi=0°)$ and (b) $I^{(2\omega)}_{\mathrm{exp},x}(\phi=45°)/I^{(2\omega)}_{\mathrm{exp},x}(\phi=0°)$ as a function of the SH photon energy for Au(887) and Au(443) surfaces. The dashed lines are the values of the ideal Au(111) surface. The solid and dashed curves are sixth-order polynomial approximations to SH experimental results, provided as guidelines to highlight the difference between the two spectra.

On the other hand, the effect of the broken symmetry due to the steps is considered to be larger for Au(443) because the density of steps is greater than on Au(887). This is consistent with the result observed in Fig. 3; that the deviation of the SH response from unity is larger for Au(443) than for Au(887). Therefore, we consider that the decrease in resonance of $I^{(2\omega)}_{\mathrm{exp},x}(\phi=90°)/I^{(2\omega)}_{\mathrm{exp},x}(\phi=0°)$ and $I^{(2\omega)}_{\mathrm{exp},y}(\phi=45°)/I^{(2\omega)}_{\mathrm{exp},x}(\phi=0°)$ from unity in the SH photon energy range from 2.5 to 3.3 eV is due to the electronic state of steps on the sample surface. However, we must be cautious here; that in order to analyze this deviation from the $3m$ symmetric response in further detail, it will be necessary to consider the contributions not only from the steps but also from the reconstructions.

Figure 4 shows the SH intensity spectra $I^{(2\omega)}_{\mathrm{exp},x}(\phi=0°)$ from Au(443) and Au(887) calibrated by α-$SiO_2(0001)$. The SH intensity tends to be larger for the lower photon energy region in both spectra. Iwai *et al.*[17] observed SHG from the Au(111) surface and the spectra exhibited stronger SH signals in a similar energy range. The SH spectrum of Au(887) in Fig. 4(b) shows a peak at the SH photon energy of 2.4 eV,

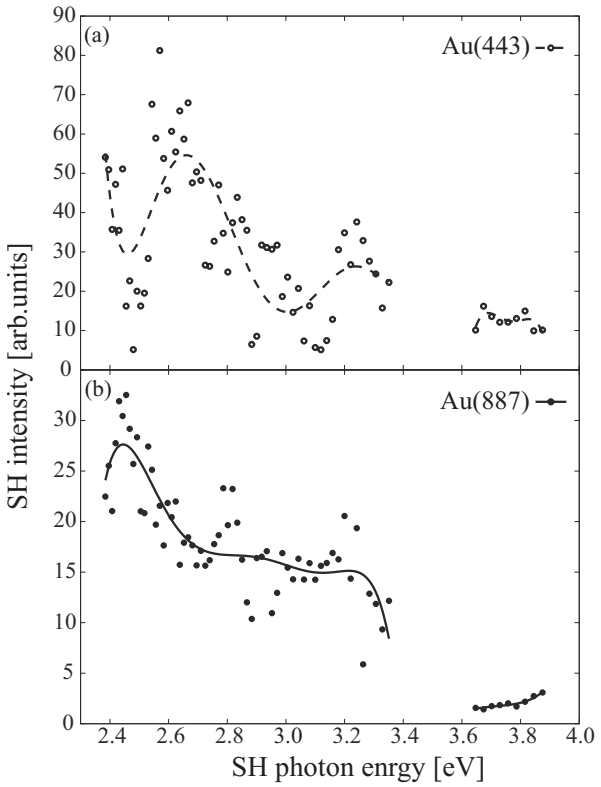

FIG. 4. The SH intensity of $I^{(2\omega)}_{\mathrm{exp},x}(\phi=0°)$ as a function of the SH photon energy for (a) Au(443) and (b) Au(887). The vertical axis is calibrated by the SH intensity from an α-SiO_2(1000) plate. The solid and dashed curves are sixth-order polynomial approximations to SH experimental results, provided as guidelines to highlight the difference between the two spectra.

similar to the data from Iwai *et al.* Otherwise the two spectra show different structures from their data. The difference between the spectra in Figs. 4(a) and 4(b) can be seen around the SH photon energy range of 2.5–3.3 eV. The origin of the difference is suggested to be the difference of the step density.

Iwai *et al.*[17] argued that the SH intensity peaks around 2.4 eV of the Au(111) and Au(100) surfaces originate from the transition from the *d*-electronic band to the *s* and *p* surface bands. Similarly, we may well say that the peak around 2.5 eV in the SH spectra of Au(443) reflects the transition from the occupied *d* electronic to the empty *s* and *p* surface bands. However, the absolute SH intensity is a function of not only the nonlinear susceptibility but also the Fresnel factors, and thus we do not analyze the detailed structures of the spectra in Fig. 4 in the present study.

In order to see the second-order nonlinear optical response of the step site in more detail, we have calculated the phase differences between the nonlinear susceptibility elements $\chi^{(2)}_{xxx}$ and $\chi^{(2)}_{xyy}$ from the experimental results. For the $3m$ symmetric Au(111) surface, $I^{(2\omega)}_{\mathrm{exp},x}(\phi=45°)/I^{(2\omega)}_{\mathrm{exp},x}(\phi=0°)$ is equal to zero, as found from Eqs. (1) and (3). However, $I^{(2\omega)}_{\mathrm{exp},x}(\phi=45°)/I^{(2\omega)}_{\mathrm{exp},x}(\phi=0°)$ is not equal to zero for Au(443) and Au(887) as can be seen in Figs. 5(a) and 5(b). The finite values of $I^{(2\omega)}_{\mathrm{exp},x}(\phi=45°)/I^{(2\omega)}_{\mathrm{exp},x}(\phi=0°)$ is due to the deviation of $|\chi^{(2)}_{xyy}/\chi^{(2)}_{xxx}|$ from unity and the phase difference between

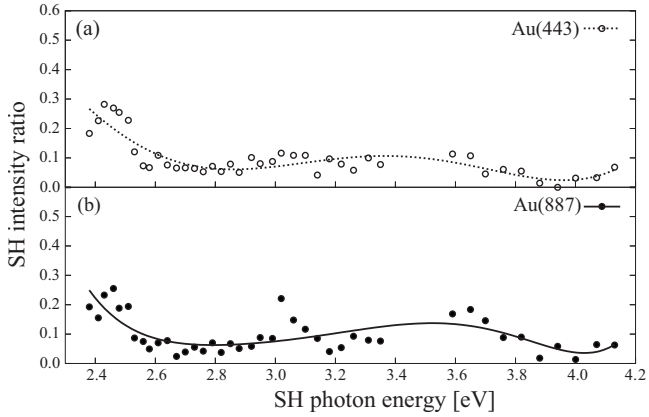

FIG. 5. The SH intensity ratios $I^{(2\omega)}_{\mathrm{exp},x}(\phi=45°)/I^{(2\omega)}_{\mathrm{exp},x}(\phi=0°)$ for (a) Au(443) and (b) Au(887). The solid and dashed curves are sixth-order polynomial approximations to SH experimental results, provided as guidelines to highlight the difference between the two spectra.

the nonlinear susceptibility elements $\chi^{(2)}_{xxx}$ and $\chi^{(2)}_{xyy}$.

Using the relations $\chi^{(2)}_{xxx}=|\chi^{(2)}_{xxx}|e^{-i\alpha}$, $\chi^{(2)}_{xyy}=|\chi^{(2)}_{xyy}|e^{-i\beta}$, and Eq. (1), we can find a relation as

$$\cos(\beta-\alpha)=2\sqrt{\frac{I^{(2\omega)}_{x,\mathrm{exp}}(0°)}{I^{(2\omega)}_{x,\mathrm{exp}}(90°)}}\left(\frac{I^{(2\omega)}_{x,\mathrm{exp}}(45°)}{I^{(2\omega)}_{x,\mathrm{exp}}(0°)}-\frac{1}{4}-\frac{1}{4}\frac{I^{(2\omega)}_{x,\mathrm{exp}}(90°)}{I^{(2\omega)}_{x,\mathrm{exp}}(0°)}\right). \tag{9}$$

Figure 6 shows the values of $\cos(\beta-\alpha)$ as a function of the SH photon energy, obtained by using Eq. (9) and the data in Figs. 3(a). In Fig. 6 we see a difference between the phases $\cos(\beta-\alpha)$ on Au(443) and Au(887), especially in the SH photon energy range from 2.5 to 3.3 eV. In the same SH photon energy range we saw dependence of $|\chi^{(2)}_{xyy}/\chi^{(2)}_{xxx}|$ and $|\chi^{(2)}_{yxy}/\chi^{(2)}_{xxx}|$ on the face index in Fig. 3.

The value $\cos(\beta-\alpha)$ is equal to -1 for a $3m$ symmetric surface from Eq. (1). The value of $\cos(\beta-\alpha)$ is closer to -1 for Au(887) than for Au(443), indicating that the phase difference $\cos(\beta-\alpha)$ also depends on the step density.

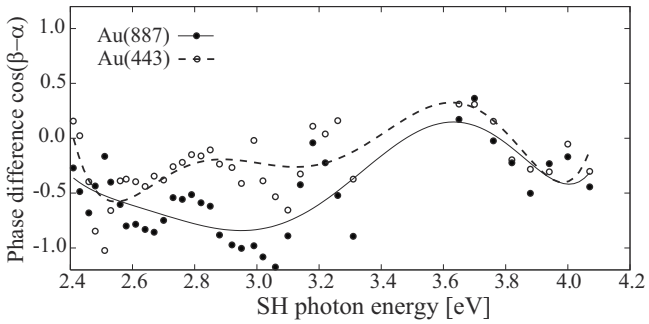

FIG. 6. The phase difference $\cos(\beta-\alpha)$ between the $\chi^{(2)}_{xxx}$ and $\chi^{(2)}_{xyy}$ elements as a function of the SH photon energy for Au(443) and Au(887). The solid and dashed curves are sixth-order polynomial approximations to SH experimental results, provided as guidelines to highlight the difference between the two spectra.

We suggest that the dependence of the absolute value of the susceptibility elements on the face index and the difference between the phases of the two susceptibility elements, $\chi^{(2)}_{xxx}$ and $\chi^{(2)}_{xyy}$, originate from the anisotropy of the local conductivity of electrons around the step site. In order to analyze the origin of the optical nonlinearity of the steps on the Au surfaces in more detail, we need to calculate the local conductivity of electrons at the step sites with a microscopic model. At present we cannot calculate the microscopic conductivity around the step site. In Sec. IV, we calculate the electronic states of stepped Au surfaces and compare them with our experimental results.

IV. CALCULATION OF THE ELECTRONIC DENSITY OF STATES ON STEPPED AU SLABS

In order to analyze the dependence of the SH intensity spectra on the surface index, we have performed a first-principles calculation of the electronic states of a vicinal Au crystalline slab with atomic steps. The slab model has Au(554) surfaces on both sides. The thickness of the unit cell in the slab was chosen to be five atomic layers because in this condition the local density of states (LDOS) of the atoms at the step, on the terrace, and in the bulk depended weakly on the thickness. In the directions parallel to the surfaces, the unit-cell size was 1×5 times that of the ideal (111) surface and the periodic boundary condition was adopted. In the direction perpendicular to the surfaces, a vacuum layer was added and the structure was repeated. When the vacuum thickness was changed from 0.4 to 0.6 nm, from 0.6 to 0.8 nm, from 0.8 to 1.0 nm, and from 1.0 to 1.2 nm, the ratios of the total energy changes were 13:4:1:1. Therefore, we chose 0.8 nm as the vacuum thickness. It was difficult for us to optimize the structure of the $\sqrt{3}\times23$ reconstructed terrace due to the large unit cell. The length of the unit cell in the direction parallel to the step edges was thus taken to be that of the bulk structure. The atomic structures were geometrically optimized before the calculation of the electronic states.

The electronic states of the Au(554) slab were calculated by the density-functional method. The exchange interaction and correlation of electrons were handled by using a generalized gradient approximation (GGA) within the Perdew-Burke-Ernzerhof (PBE) scheme. A double numerical plus polarization (DNP) basis set was used. The calculations were conducted using the code named DMol3 in Materials Studio (ACCELRYS, version 4.2).[18–20]

From the obtained Kohn-Sham orbitals, the *d* partial density of states at three atomic sites in the bulk [Fig. 7(a)], on the terrace [Fig. 7(b)], and on the step [Fig. 7(c)] were calculated. These three sites are schematically illustrated in the insets in Fig. 7. The solid curve in Fig. 7(d) shows the difference between the *d* partial density of states of the step atom [Fig. 7(c)] and the terrace atom [Fig. 7(b)], and the dashed curve shows the difference between the terrace atom [Fig. 7(b)] and the bulk atom [Fig. 7(a)]. The calculated *s* and *p* partial density of states of the step, terrace, and bulk atoms are widely spread from −8 to 3 eV. The differences in *s* and *p* between the different atomic sites are much smaller than those for the *d* partial density of states and are not shown here.

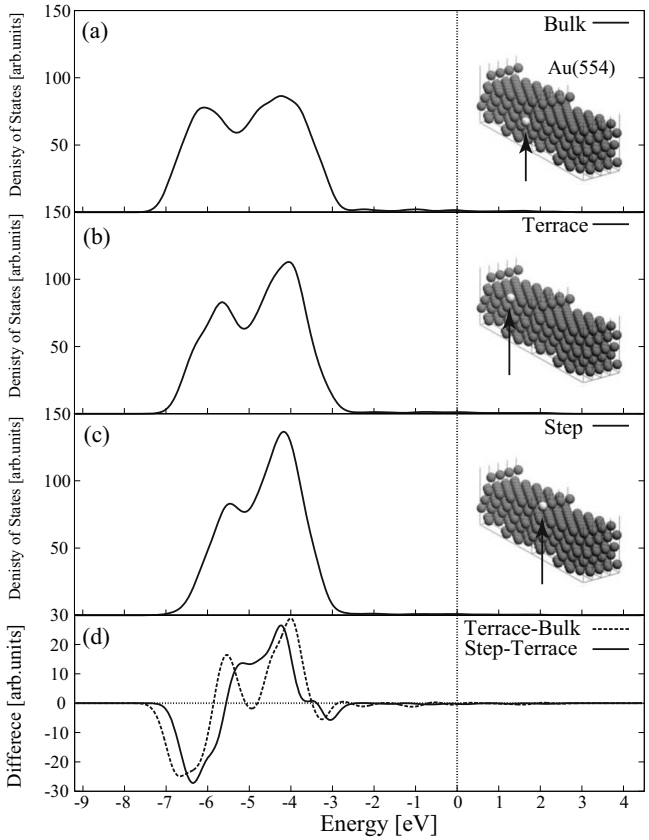

FIG. 7. The *d* partial electronic density of states of Au atoms (a) in the bulk, (b) on the terrace, and (c) on the step, obtained from DFT calculation of a Au (554) slab consisting of five atomic layers. The solid curve in (d) indicates the difference between the *d* partial electronic density of states of the Au atoms on the step and those on the terrace. The dashed curve indicates the difference between the Au atoms on the terrace and in the bulk. Fermi level corresponds to 0 eV.

In Fig. 7 we see that the 5*d* partial density of states of the step and the terrace differ from each other below the energy of −2.5 eV. The SH intensity ratios $I^{(2\omega)}_{\mathrm{exp},x}(\phi=90°)/I^{(2\omega)}_{\mathrm{exp},x}(\phi=0°)$ in Fig. 3(a) gradually split between the Au(443) and Au(887) surfaces above the SH photon energy of 2.5 eV and so do those of $I^{(2\omega)}_{\mathrm{exp},x}(\phi=45°)/I^{(2\omega)}_{\mathrm{exp},x}(\phi=0°)$ in Fig. 3(b).

The SH intensity is a function of the transition moments between the electronic states involved in the optical process, relaxation constants of the states, Fresnel factors, and LDOS. The first three parameters are seen to be weakly dependent on the photon energy for the following reasons.

The main term in the second-order nonlinear optical susceptibility is given as

$$\chi^{(2)}_{ijk}(-2\omega;\omega,\omega)\propto\sum_{lmf}\frac{\langle l|\mu_i|f\rangle\langle f|\mu_j|m\rangle\langle m|\mu_k|l\rangle}{(2\hbar\omega-E_{fl}-i\hbar\gamma_{fl})(\hbar\omega-E_{ml}-i\hbar\gamma_{ml})}, \tag{10}$$

where $|l\rangle$, $|m\rangle$, and $|f\rangle$ represent the initial, intermediate, and final electronic states, respectively, in the three-photon process.[14] If we limit ourselves to the case of a specific resonance, the electronic states $|l\rangle$, $|m\rangle$, and $|f\rangle$ in Eq. (10) can be assumed as specific. Consequently, the transition moments

$\langle l|\mu_i|f\rangle$, $\langle f|\mu_j|m\rangle$, and $\langle m|\mu_k|l\rangle$ are roughly constant.

In the denominator of Eq. (10) γ_{fl} and γ_{ml} are relaxation constants of the states. These relaxation constants can be regarded as constant if one specific resonance is considered.[21]

If we further assume that only the photon energy $2\hbar\omega$ is resonant with electronic levels, Eq. (10) is roughly proportional to the sum of Lorentzian terms of width $\hbar\gamma_{fl}$ related to the transition from $|f\rangle$ to $|l\rangle$ states. Then the whole equation is roughly proportional to the joint density of states (JDOS) between the states of $|l\rangle$ and $|f\rangle$.

Our discussion focuses on the onset of the deviation of the SH response from the $3m$ symmetric pattern near 2.5 eV. In this energy range the linear optical response, such as the optical reflectance of Au, varies moderately so that the variation of the Fresnel factors can be regarded as sufficiently moderate compared to the steepness of the onset of the SH response of the steps, as sharp as 0.1 eV. Under the above assumptions the SH intensity should be roughly proportional to the square of the joint density of states for the two-photon transition between the occupied d-electronic states and the empty s and p states just above the Fermi level. Thus the resonance with the two-photon transition from the d-bands to the s and p bands at the step should enlarge the nonlinear susceptibility $\chi^{(2)}_{\text{step}}$. By this $\chi^{(2)}_{\text{step}}$ the SH response originating from $\chi^{(2)}_{3m}+\chi^{(2)}_{\text{step}}$ is modulated through interference.

Since the binding energy at the onset of the undulation of the solid curve (−2.5 eV) in Fig. 7(d) is roughly equal to the onset energy of the splitting in Fig. 3, we suggest that the splitting of the SH intensity ratios in Fig. 3 is due to the modification of the LDOS of the d electrons by the steps. Because the Au(443) surface has step bunching, unlike the Au(887) surface, the SH intensity should not simply be proportional to the step density so far as our two samples are concerned.

On the high-energy side, in Fig. 3, the results suggest the contribution of the electrons at the step is smaller in the SH response because it does not show dependency on the face index. Candidate reasons for this disappearance of the splitting would be the decrease in the joint density of states and the dipole transition moments, and the increase in the relaxation rate at the step sites. On the other hand, there also should be a reason why the SH intensity ratios $I^{(2\omega)}_{\text{exp},x}(\phi=90°)/I^{(2\omega)}_{\text{exp},x}(\phi=0°)$ and $I^{(2\omega)}_{\text{exp},x}(\phi=45°)/I^{(2\omega)}_{\text{exp},x}(\phi=0°)$ are still far from unity, around 3.7 eV in Fig. 3. The broken symmetry caused by the reconstruction on the terraces is one possibility. The details are not clear yet and calculation of the reconstructed surface is required for further discussion.

V. CONCLUSION

Reflected SH spectroscopy with normal incidence was performed for Au(443) and Au(887). A difference in SH intensity patterns between Au(443) and Au(887) was detected around the SH photon energy in the 2.5–3.3 eV range. This difference originates from the broken symmetry caused by the periodic steps on the vicinal surfaces. Phase differences between the nonlinear susceptibility elements $\chi^{(2)}_{xxx}$ and $\chi^{(2)}_{xyy}$ were also found to depend on the face index in the SH photon energy range from 2.5 to 3.3 eV.

We performed a first-principles calculation to determine the electronic density of states of a stepped Au(111) slab consisting of five atomic layers. The calculation showed a difference in the d partial density of states between the atoms at the step and terrace sites for a binding energy larger than 2.5 eV. This result suggests that one of the reasons for the dependency of SH intensity on the surface index is the contribution of the d electrons at the steps.

ACKNOWLEDGMENTS

The authors would like to thank T. Shimoda, Dam Hieu Chi, and A. Sugiyama for their support in the theoretical calculations.

*Corresponding author. mizutani@jaist.ac.jp

[1] B. Hammer and J. K. Norskov, Nature (London) **376**, 238 (1995).
[2] M. Ruff, S. Frey, B. Gleich, and R. J. Behm, Appl. Phys. A: Mater. Sci. Process. **66**, S513 (1998).
[3] M. Date, Y. Ichihashi, T. Yamashita, A. Chiorino, F. Boccuzzi, and M. Haruta, Catal. Today **72**, 89 (2002).
[4] M. Haruta, N. Yamada, T. Kobayashi, and S. Iijima, J. Catal. **115**, 301 (1989).
[5] M. Valden, X. Lai, and D. W. Goodman, Science **281**, 1647 (1998).
[6] M. Mavrikakis, P. Stoltze, and J. K. Norskov, Catal. Lett. **64**, 101 (2000).
[7] J. E. Ortega, A. Mugarza, V. Repain, S. Rousset, V. Perez-Dieste, and A. Mascaraque, Phys. Rev. B **65**, 165413 (2002).
[8] S. Shiraki, H. Fujisawa, M. Nantoh, and M. Kawai, J. Electron Spectrosc. Relat. Phenom. **137-140**, 177 (2004).
[9] S. Rousset, F. Pourmir, J. M. Berroir, J. Klein, J. Lecoeur, P. Hecquet, and B. Salanon, Surf. Sci. **422**, 33 (1999).
[10] S. Rohart, Y. Girard, Y. Nahas, V. Repain, G. Rodary, A. Tejeda, and S. Rousset, Surf. Sci. **602**, 28 (2008).
[11] T. Kitahara, H. Tanaka, Y. Nishioka, and G. Mizutani, Phys. Rev. B **64**, 193412 (2001).
[12] S. Janz, D. J. Bottomley, H. M. van Driel, and R. S. Timsit, Phys. Rev. Lett. **66**, 1201 (1991).
[13] N. Takeuchi, C. T. Chan, and K. M. Ho, Phys. Rev. B **43**, 13899 (1991).
[14] P.-F. Brevet, *Surface Second Harmonic Generation* (Presses Polytechniqnes et Universitaires Romandes, Lausanne, 1997), p. 43.
[15] L. Piccolo, D. Loffreda, F. J. Cadete Santos Aires, C. Dranlot, Y. Jugnet, P. Sautet, and J. C. Bertolini, Surf. Sci. **566-568**, 995 (2004).
[16] J. E. Sipe, D. J. Moss, and H. M. van Driel, Phys. Rev. B **35**, 1129 (1987).
[17] T. Iwai and G. Mizutani, Phys. Rev. B **72**, 233406 (2005).
[18] B. Delley, J. Chem. Phys. **92**, 508 (1990).
[19] B. Delley, J. Chem. Phys. **113**, 7756 (2000).
[20] http://www.accelrys.com/
[21] Charles Kittel, *Introduction to Solid State Physics*, 7th ed. (Wiley, New York, 1998).